Fragment yield distribution and the influence of neutron composition and excitation energy in multifragmentation reactions

D. V. Shetty,[1] A. S. Botvina,[1,2] S. J. Yennello,[1] G. A. Souliotis,[1] E. Bell,[1] and A. Keksis[1]
[1]*Cyclotron Institute, Texas A&M University, College Station, TX 77843*
[2]*Institute for Nuclear Research, 117312 Moscow, Russia*
(Received 14 September 2004; published 2 February 2005; publisher error corrected 4 February 2005)

The isotopic properties of the primary and secondary fragment yield distribution in the multifragmentation of ^{58}Fe + ^{58}Ni and ^{58}Fe + ^{58}Fe reactions are studied with respect to the ^{58}Ni + ^{58}Ni reaction at 30, 40, and 47 MeV/nucleon. The reduced neutron and proton densities from the observed fragment yield distribution show primary fragment yield distribution to undergo strongly secondary deexcitations. The effect is small at the lowest excitation energy and smallest neutron-to-proton ratio and becomes large at higher excitation energies and higher neutron-to-proton ratio. The symmetry energy of the primary fragments deduced from the reduced neutron density is significantly lower than that for the normal nuclei at saturation density, indicating that the fragments are highly excited and formed at a reduced density. Furthermore, the symmetry energy is also observed to decrease slowly with increasing excitation energy. The observed effect is explained using the statistical multifragmentation model.

DOI: 10.1103/PhysRevC.71.024602 PACS number(s): 25.70.Mn, 25.70.Pq, 26.50.+x

I. INTRODUCTION

In multifragmentation reactions an excited nuclei expand into vacuum and decay into various light and heavy fragments [1–4]. These fragments when emitted are highly excited and neutron-rich and subsequently undergo deexcitation to cold and stable isotopes. Similar hot nuclei are also produced in the interior of a collapsing star and subsequent supernova explosion [5]. The production of these nuclei depends on their internal excitation and is sensitive to the symmetry energy part of the binding energy [6]. A slight decrease in the symmetry energy coefficient and subsequent deexcitation can significantly alter the elemental abundance and the synthesis of heavy elements [5]. In multifragmentation reactions the measurement of fragment isotopic yield distribution can provide important insight into the symmetry energy and the decay characteristics of these nuclei.

Experimentally, the determination of fragment isotopic yield distribution is often influenced by the complex deexcitation of the primary fragments to their finally observed secondary yield distribution. Theoretical calculations of the yields after secondary deexcitations require an accurate accounting of the feeding from the particle unstable state and are subject to uncertainties in the levels that can be excited and the structure effects that govern their decay.

In this work, we study the primary fragment yield distribution and the associated symmetry energy through relative reduced neutron and proton densities at various excitation energy and isospin (N/Z) of the multifragmenting source. It has been shown [7] that the relative reduced neutron and proton densities can provide an alternate way of studying the isotopic yield distribution, where some of the uncertainties mentioned above can be avoided by taking the ratios of the yield in two different reactions that differ only in their isospin (N/Z) content. Also, the reduced neutron density is directly related to the symmetry energy through a scaling relation as discussed in [6,8–10].

In this work we show that the primary fragment yield distribution is strongly affected by the secondary deexcitations at higher excitation energies and isospin (N/Z) of the fragmenting system. The symmetry energy of the primary fragments deduced from the scaling parameter is considerably lower than that for the saturation value and decreases with increasing excitation energy. The observed effect can be well explained by the statistical multifragmentation model of Botvina *et al.* [6].

II. EXPERIMENT

The measurements were carried out at the Cyclotron Institute of Texas A&M University (TAMU) using beams from the K500 Superconducting Cyclotron. Isotopically pure beams of ^{58}Ni and ^{58}Fe at 30, 40, and 47 MeV/nucleon were bombarded on self-supporting ^{58}Ni (1.75 mg/cm^2) and ^{58}Fe (2.3 mg/cm^2) targets. Six discrete particle telescopes placed inside a scattering chamber at laboratory angles of 10°, 44°, 72°, 100°, 128°, and 148° were used to measure the fragments from the reactions. Each telescope consisted of a gas ionization chamber (IC) followed by a pair of silicon detectors (Si-Si) and a CsI scintillator detector, providing three distinct detector pairs (IC-Si, Si-Si, and Si-CsI) for fragment identification. The ionization chamber was of axial field design and was operated with CF_4 gas at a pressure of 50 torr. The gaseous medium was 6 cm thick with a typical threshold of ∼0.5 MeV/A for intermediate mass fragments. The silicon detectors had an active area of 5 cm × 5 cm and were each subdivided into four quadrants. The first and second silicon detectors in the stack were 0.14 and 1 mm thick, respectively. The dynamic energy range of the silicon pair was ∼16–50 MeV for ^{4}He and ∼90–270 MeV for ^{12}C. The CsI scintillator crystals that followed the silicon detector pair were 2.54 cm in thickness and were read out by photodiodes. Good Z identification was achieved for fragments that punched through the IC detector and stopped in the first silicon detector. Fragments measured

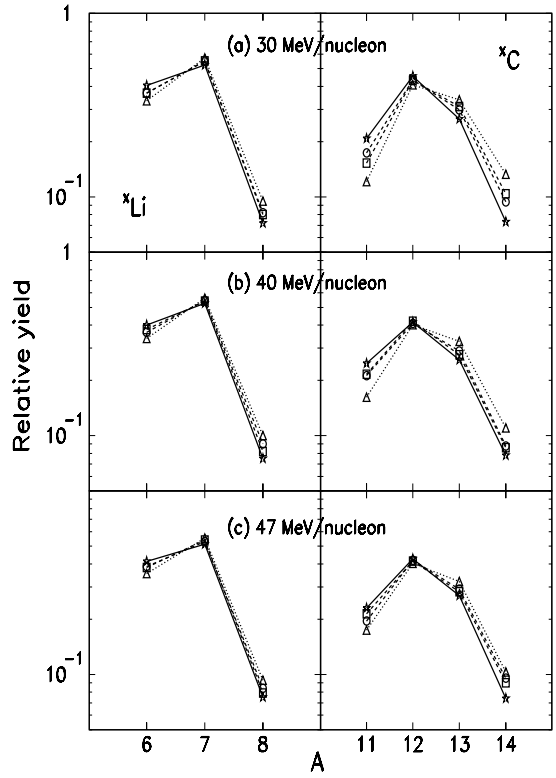

FIG. 1. Relative yield distribution of the fragments for the lithium (left) and carbon (right) isotopes in ^{58}Fe + ^{58}Fe, ^{58}Fe + ^{58}Ni, ^{58}Ni + ^{58}Fe, and ^{58}Ni + ^{58}Ni reactions at three different beam energies. The different symbols are for the four reactions as discussed in the text.

in the Si-Si detector pair also had good isotopic separation. Further details can be found in Refs. [11,12].

The present study is carried out for fragments detected at 44° in the laboratory system, which corresponds to the center of mass angle ≈90°. The fragments detected at this angle originate predominantly from central events which was further assured by gating on the measured neutron multiplicities. A possible admixture of the projectile/target fragmentation processes will nevertheless be accounted for in the following analysis. Figure 1 shows the experimentally determined yield distributions for the lithium (left panels) and carbon (right panels) isotopes measured in ^{58}Fe + ^{58}Fe (triangle symbols), ^{58}Fe + ^{58}Ni (circle symbols), ^{58}Ni + ^{58}Fe (square symbols), and ^{58}Ni + ^{58}Ni (star symbols) reactions at the three different beam energies. The data show the highest yield for the neutron-rich isotopes in the ^{58}Fe + ^{58}Fe reaction (triangles), which has the largest neutron-to-proton ratio (N/Z), compared to the ^{58}Ni + ^{58}Ni reaction (stars), which has the smallest neutron-to-proton ratio. The yields for the reactions with the intermediate value of the neutron-to-proton ratio, ^{58}Ni + ^{58}Fe (squares) and ^{58}Fe + ^{58}Ni (circles) lie in between. One also observes that the difference in the yield distribution for the four reactions decreases with increasing beam energy. As will become evident in the following sections, this is a consequence of the secondary deexcitation of the primary fragments that becomes dominant for systems with increasing neutron-to-proton ratio and excitation energy.

III. THE REDUCED NUCLEON DENSITIES

Using the experimentally observed yield distribution, the reduced neutron and proton densities were extracted as follows. In a Grand-Canonical approach for the multifragmentation process (see, e.g., [13–16]), the fragment yield for an isotope with neutron number N and proton number Z (mass number $A = N + Z$) is given as follows:

$$Y(N, Z) \propto V \rho_n^N \rho_p^Z Z_{N,Z}(T) A^{3/2} e^{B(N,Z)/T}, \tag{1}$$

where V is the volume of the system and $\rho_n \propto e^{\mu_n/T}$ and $\rho_p \propto e^{\mu_p/T}$ are the primary "free" neutron and proton densities, respectively. The exponents μ_n and μ_p are the neutron and the proton chemical potentials, and $Z_{N,Z}(T)$ is the intrinsic partition function of the excited fragment. The quantity $B(N, Z)$ is the ground-state binding energy of the fragment and T is the temperature. In the above formula, the effect of the Coulomb interaction on fragment yield is often neglected. By introducing ρ_n and ρ_p, the actual isotope yields are reduced to an approximation appropriate for the thermodynamical limit at high excitation energies [13]. Hence, they are referred to as the "reduced" densities.

As discussed in the introduction, taking the ratios of the fragment yield from two different systems that differ only in their isospin (N/Z) content reduces the uncertainties in the quantities shown in Eq. (1). For the present analysis all ratios were taken with respect to the least neutron-rich ^{58}Ni + ^{58}Ni reaction. The isotopic yield distribution of the fragments in terms of relative reduced neutron density is then given as follows:

$$\frac{Y(N+k, Z)/Y^{Ni+Ni}(N+k, Z)}{Y(N, Z)/Y^{Ni+Ni}(N, Z)} = \left(\frac{\rho_n}{\rho_n^{Ni+Ni}}\right)^k, \tag{2}$$

where k corresponds to the different isotopes used to determine the double ratio and Y^{Ni+Ni} is the yield for the ^{58}Ni + ^{58}Ni reaction. A similar expression for the relative reduced proton density from the isotonic yield ratios can also be written as follows:

$$\frac{Y(N, Z+k)/Y^{Ni+Ni}(N, Z+k)}{Y(N, Z)/Y^{Ni+Ni}(N, Z)} = \left(\frac{\rho_p}{\rho_p^{Ni+Ni}}\right)^k, \tag{3}$$

Figure 2 (symbols) shows the relative reduced neutron and proton densities as a function of excitation energy (which correspond to different beam energies as discussed in the next section) of the fragmenting source for the ^{58}Fe + ^{58}Ni and ^{58}Fe + ^{58}Fe reactions. The various symbols in the figure correspond to the densities obtained using $k = 1$, $k = 2$, and $k = 3$ for various isotopes and isotones. The figure shows a steady decrease in the reduced neutron density and an increase in the proton density with increasing excitation energy. The effect is stronger for the ^{58}Fe + ^{58}Fe reaction, which has the highest isospin (N/Z) content.

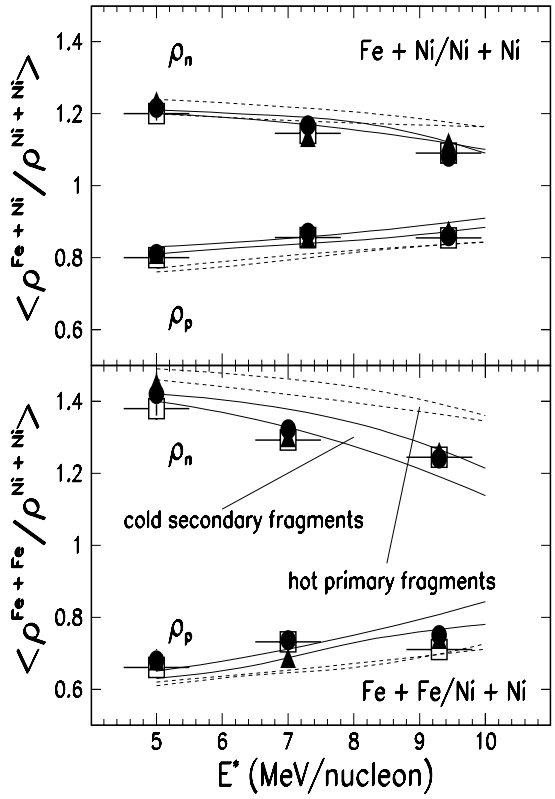

FIG. 2. Experimentally determined relative reduced neutron and proton densities as a function of excitation energy for the ^{58}Fe + ^{58}Ni and ^{58}Fe + ^{58}Fe reactions with respect to the ^{58}Ni + ^{58}Ni reaction. The regions bounded by the solid and the dotted lines are the statistical model calculations for the cold secondary and hot primary fragments, respectively, and are explained in the text.

IV. COMPARISON OF THE REDUCED NUCLEON DENSITIES WITH THE STATISTICAL MULTIFRAGMENTATION MODEL CALCULATION

To study the effect of secondary deexcitation at various excitation energies and isospin content (N/Z) of the fragmenting system, a comparison of the observed reduced neutron and proton densities with the statistical multifragmentation model (SMM) of Botvina *et al*. [6] was carried out. The initial parameters for the SMM calculation, such as the mass (A_s), charge (Z_s), and excitation energy (E_s^*) of the thermal source, were estimated by simulating the initial stage of the collision dynamics using the Boltzmann-Nordheim-Vlasov (BNV) model calculation [17]. The parameters obtained for the ^{58}Fe + ^{58}Ni reaction are $A_s \approx 111$, $Z_s \approx 52$, and $E_s^* \approx 5$, 7, and 9.4 MeV/nucleon for the three beam energies studied. The N/Z ratios of the sources in all cases were not very different from those of the interacting nuclei. These results were obtained at a time around 40–50 fm/c after the projectile fuses with the target nuclei and the quadrupole moment of the nucleon coordinates (used for identification of the deformation of the system) nearly goes to zero. Also, the form of single source in the calculation oscillates throughout the dynamical evolution and does not undergo any dynamical disintegration, assuring that the dynamical flow produced in these reactions are insignificant for the energies studied.

The source parameters were also compared with the experimental data of Hudan *et al*. [18], where a nearly symmetric central collisions of Xe + Sn was studied and an excitation energy of ≈5 MeV/nucleon at 32 MeV/nucleon and ≈7 MeV/nucleon at 50 MeV/nucleon was obtained. It was shown in this work that the SMM calculation describes the disassembly of these systems and the excitation energies of the observed primary fragments quite well. A radial flow of ≈2 MeV/nucleon was, however, identified in this case for the 50 MeV/nucleon beam energy. In the present case, the systems are twice as small and stable. Further, it is obvious from various measurements (see, e.g., [19]) that smaller systems accumulate smaller radial flow than larger systems. Consequently, a large part of the energy becomes available in the form of thermal excitation.

To account for the possible uncertainties in the source parameters due to loss of nucleons during preequilibrium emission and the sensitivity of the final results toward the source size, the calculations were also performed for smaller source sizes of $A_s = 58$ with $Z_s = 26, 27,$ and 28. The freeze-out density in the calculation was assumed to be 1/3 of the normal nuclear density and the deexcitation of the hot primary fragments was carried out via evaporation, fission or Fermi breakup [16].

Figure 3 shows the mean characteristics of the hot primary fragments in the freeze-out volume calculated from the statistical multifragmentation model. Shown are their relative yields, internal excitation energies, and N/Z ratios as a function of their mass. At the lowest excitation energy $E_s^* = 6$ AMeV, the primary fragments are characterized by an exponential-like mass distribution (bottom panel). With increasing excitation of the source the internal excitation energy of the fragments increases and the source breaks up into smaller fragments. For sources with different neutron-to-proton ratios (N/Z), the primary fragments are also produced with varying N/Z ratios depending on the source excitation energy (top panel).

The characteristics of the hot primary fragments, however, change significantly after the secondary deexcitation as shown in Fig. 4. Both the mass and the neutron content of the cold secondary fragments decrease considerably lowering the N/Z ratio because of a higher evaporation probability of neutrons relative to protons. The N/Z of the light fragments vary with Z reflecting their shell structure. However, the qualitative difference between the N/Z ratios of the hot fragments (middle panel) produced by the sources with different isospin remains the same even after the secondary deexcitation, although it becomes smaller. Moreover, one can see the solid and the dotted lines in the middle panel to be more distinguished than those in Fig. 3. The average difference between the cases with the two excitations increases from 0.0051 to 0.0168 for the fragments $A = 6$–20. This means that the difference in the N/Z of the fragments produced between the neutron-rich and the neutron-poor sources decreases more rapidly for high excitation energies as a result of more intensive secondary deexcitation.

Figure 2 presents the comparison between the experimentally (symbols) determined relative reduced neutron and

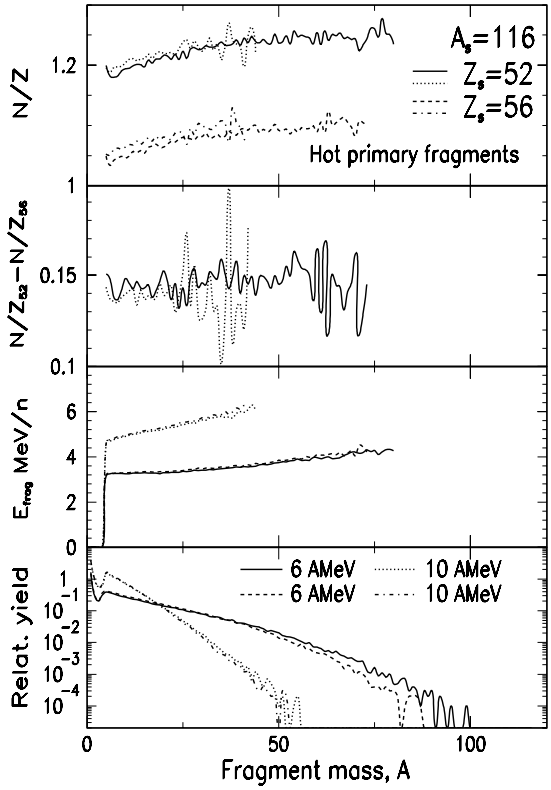

FIG. 3. Characteristics of the hot primary fragments versus their mass number A, produced in the freezeout volume during multifragmentation of the thermal sources, with mass number $A_s = 116$ and charges $Z_s = 52$ and $Z_s = 56$ at excitation energies of $E_s^* = 6$ and 10 MeV/nucleon (see notations in the figure). (Panels from top to bottom) Neutron to proton (N/Z) ratio; difference of N/Z ratios between neutron rich ($Z_s = 52$) and neutron poor ($Z_s = 56$) sources at different E_s^*; internal excitation energies; relative mass yields.

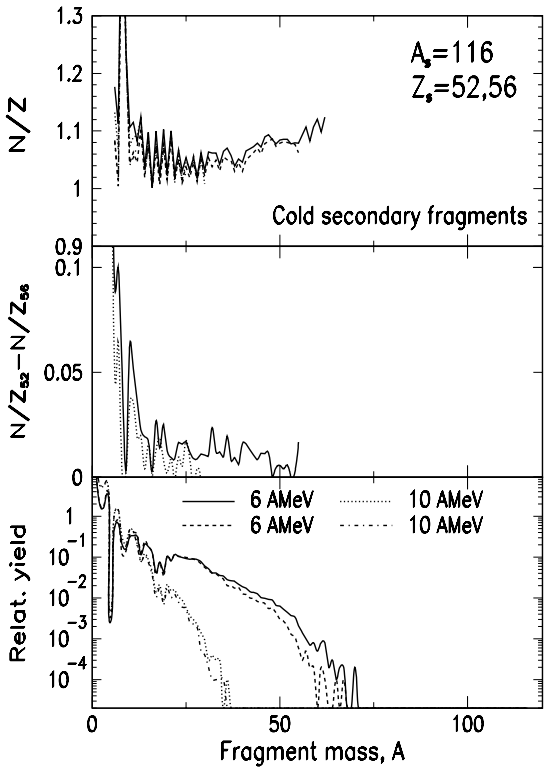

FIG. 4. Same as in Fig. 3, but for the cold fragments produced after the secondary deexcitation of the primary fragments.

proton densities and the calculations from the statistical multifragmentation model (lines). The regions enclosed between the solid lines correspond to the SMM calculation obtained from the secondary fragment yield distribution, and those between the dotted lines correspond to the densities obtained from the primary fragment yield distribution. The width of the two regions represents an upper limit to the sensitivity of the calculation to the assumed source size as discussed in Sec. IV. The error bars for the excitation energies (horizontal lines) correspond to two different equations of state used in the BNV calculation, namely the asy-stiff and the asy-soft equations of state. It is observed that the statistical multifragmentation model calculation from the secondary fragment yield distribution explains the observed data quite well. The calculated densities from the primary and the secondary fragment distribution are not very different for the ^{58}Fe + ^{58}Ni reaction. But those for the ^{58}Fe + ^{58}Fe reaction, which has a higher neutron-to-proton (N/Z) content, are significantly different. The difference is small at a lower excitation energy and becomes larger with increasing excitation energy. The comparison shows that the primary fragment yield distribution for systems with a large neutron-to-proton (N/Z) ratio and initial excitation energy are strongly affected by the secondary deexcitation process. With increasing excitation energy and neutron-to-proton ratio of the fragmenting system, the primary fragments are highly neutron rich and produced with large internal excitation energy that quickly undergoes secondary deexcitation leading to a decrease in the width of the yield distribution as observed in Fig. 1. Such an effect has also been observed for fragments produced in a dynamical stochastic mean-field calculation [17,20].

V. THE REDUCED NEUTRON DENSITY AND THE SYMMETRY ENERGY

In the following, we extract the symmetry energy of the primary fragments from the reduced neutron density and study their dependence on the excitation energy of the fragmenting system. From Eq. (1) the ratio of the fragment yield from two different reactions can be written as follows:

$$\frac{Y(N,Z)}{Y^{Ni+Ni}(N,Z)} = C\left(\frac{\rho_n}{\rho_n^{Ni+Ni}}\right)^N \left(\frac{\rho_p}{\rho_p^{Ni+Ni}}\right)^Z = C\hat{\rho}_n^N \hat{\rho}_p^Z, \tag{4}$$

where C is the overall normalization factor and $\hat{\rho}_n$, $\hat{\rho}_p$ are the relative reduced neutron and proton densities. The relative reduced neutron and proton densities are related to the isoscaling parameters $\alpha = \Delta\mu_n/T$ and $\beta = \Delta\mu_p/T$ through a relationship given by $e^\alpha = \hat{\rho}_n$ and $e^\beta = \hat{\rho}_p$. The quantities $\Delta\mu_n$ and $\Delta\mu_p$ are the difference in the neutron and the proton chemical potential between the two reactions. The parameter α is related to the symmetry energy part of the fragment binding

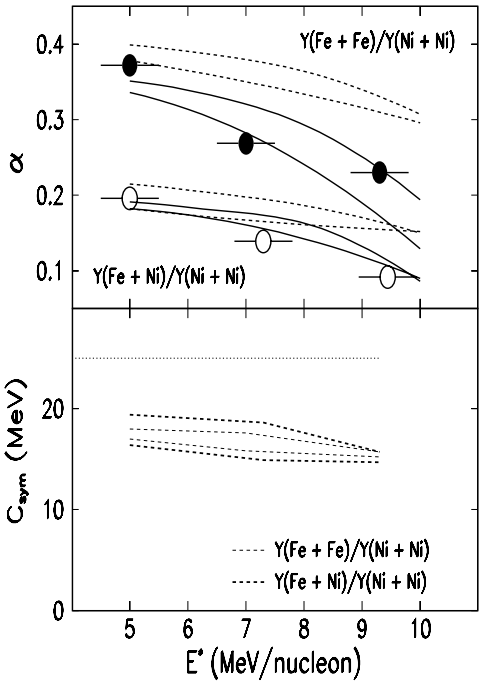

FIG. 5. Isoscaling parameter (top) and symmetry energy (bottom) as a function of excitation energy of the fragmenting source for the ^{58}Fe + ^{58}Ni and ^{58}Fe + ^{58}Fe reactions. (Top) The dashed and the solid curves are the calculated values of α from the primary and secondary fragment yield distributions using SMM, respectively. (Bottom) Symmetry energy calculated using the primary fragment yield distribution.

energy $C_{\rm sym}$ and given as follows (see Ref. [6]):

$$\alpha T = 4C_{\rm sym}\left(\frac{Z_1^2}{A_1^2} - \frac{Z_2^2}{A_2^2}\right), \tag{5}$$

where Z_1, A_1 and Z_2, A_2 are the charge and the mass numbers of the fragmenting systems. Figure 5 (top panel) shows the experimentally determined (symbols) isoscaling parameter α from the reduced neutron density as a function of excitation energy of the fragmenting system. Also shown in the figure are the calculated values of the scaling parameter from the primary (dashed curve) and the secondary (solid curve) fragment yield distribution using the statistical multifragmentation model. Within the uncertainties in the input parameters of the SMM calculation, the decrease in the α values with increasing excitation energy is well explained by the calculation once the secondary deexcitation effect in the primary distribution is taken into account. Also, the calculated values from the secondary fragment distribution are not very different from those calculated from the primary fragment distributions for the lower excitation energies. However, with increasing excitation energy and isospin (N/Z) of the system they differ significantly. More specifically, the scaling parameter α for the neutron-rich primary fragments produced at excitation energies greater than 5–6 MeV/nucleon are strongly affected by the secondary decay effect.

Having demonstrated the fact that the observed scaling parameter is well reproduced by the statistical multifragmentation model and that a high degree of thermalization is expected during the fragment formation, we have attempted to obtain an estimate of the symmetry energy $C_{\rm sym}$ of the primary fragments using Eq. (5). The temperature for the estimate was determined using the double isotope ratio of the fragment yield [14]. Because the determination of the temperature from the fragment yield is also affected by the secondary deexcitation, a maximum correction of 70% was applied to be consistent with the previous determination of temperature for similar reactions (see Ref. [21]). This correction results in a temperature value of 6–7 MeV over the energy range studied. The difference $(Z/A)_1^2 - (Z/A)_2^2$ of the fragmenting system was estimated at $t = 50$ fm/c using the dynamical model calculations [10,17,22] and was about a 3% lower than the difference in the initial Z/A of the systems. Within these uncertainties, one obtains $C_{\rm sym}$ between 15 and 20 MeV over the excitation energy range studied. The estimated values from both the systems, ^{58}Fe + ^{58}Fe and ^{58}Fe + ^{58}Ni, are comparable to each other and shown by the thin and thick dashed lines in Fig. 5 (bottom). These observed values are significantly lower than the standard value of 25 MeV (dotted line) often assumed for a stable and unexcited nuclei. Furthermore, the symmetry energy is also observed to decrease slowly with increasing excitation energy. It should be mentioned that the estimated value of the symmetry energy is sensitive to the corrections assumed for the $(Z/A)_1^2 - (Z/A)_2^2$ in Eq. (5). A lower value of the $(Z/A)_1^2 - (Z/A)_2^2$ could raise the value of symmetry energy. An uncertainity in $(Z/A)_1^2 - (Z/A)_2^2$ of 30% could increase the symmetry energy value to about 19–20 MeV. However, it would require a correction of more than 70% at the highest excitation energy to reproduce the standard value of 25 MeV. Such an increase in not supported by any dynamical calculations and appears unlikely. It thus appears impossible to reproduce the standard value of the symmetry energy by any means. The data along with the calculations thereby suggests that the symmetry energy is below 20 MeV and well below the standard value. The reduced value of the symmetry energy shows that the primary fragments are not only excited and neutron rich but also expand to a reduced density when formed. For higher excitation energies the fragments appear to expand to even lower symmetry energies. A self-consistent check of the SMM calculation shows strong variations in the properties of the primary fragments when $C_{\rm sym}$ is varied in the range 15–25 MeV. Recently [5], it has been shown that neutron-rich hot nuclei can be produced in stellar matter between the protoneutron star and the shock front in a type II supernova explosion. In particular, it has been shown that a slight decrease in the symmetry energy coefficient can shift the mass distributions to higher masses. This property of hot nuclei could thus be interesting to investigate for understanding the relative abundance of elements in the core collapse supernovae explosion.

VI. CONCLUSION

In conclusion, we have studied the isotopic properties of the primary and secondary fragment yield distribution using the reduced nucleon densities in multfragmentation

of ^{58}Ni + ^{58}Ni, ^{58}Fe + ^{58}Ni, and ^{58}Fe + ^{58}Fe reactions at 30, 40, and 47 MeV/nucleon. It is shown that the primary fragment yield distribution for a system with a large excitation energy and neutron-to-proton ratio are significantly affected by the secondary deexcitation effects. The effect is small at lower excitation energy and smaller neutron-to-proton ratio and becomes large with increasing excitation and neutron-to-proton ratio. The symmetry energy for the fragments deduced from the scaling parameter after correcting for the secondary decay effect is considerably lower than the standard value at saturation density. Furthermore, the symmetry energy decreases with increasing excitation energy, indicating that the fragment nuclei are hot and expand to a reduced density when formed. The present observation could be important in the understanding of the mechanism of the core collapse supernovae explosions and the relative abundance of the produced elements.

ACKNOWLEDGMENT

The authors thank the staff of the Texas A&M Cyclotron facility for the excellent beam quality. This work was supported in part by the Robert A. Welch Foundation through Grant No. A-1266 and the Department of Energy through Grant No. DE-FG03-93ER40773. One of the authors (ASB) thanks Cyclotron Institute TAMU for hospitality and support.

[1] B. Borderie *et al*., Phys. Rev. Lett. **86**, 3252 (2001).
[2] D. R. Bowman *et al*., Phys. Rev. Lett. **67**, 1527 (1991).
[3] M. D'Agostino *et al*., Phys. Lett. **B371**, 175 (1996).
[4] L. Beaulieu *et al*., Phys. Rev. Lett. **84**, 5971 (2000).
[5] A. S. Botvina and I. N. Mishustin, Phys. Lett. **B584**, 233 (2004).
[6] A. S. Botvina, O. V. Lozhkin, and W. Trautmann, Phys. Rev. C **65**, 044610 (2002).
[7] H. Xu *et al*., Phys. Rev. Lett. **85**, 716 (2000).
[8] M. B. Tsang *et al*., Phys. Rev. C **64**, 054615 (2001).
[9] E. Geraci *et al*., Nucl. Phys. **A732**, 173 (2001).
[10] A. Ono *et al*., Phys. Rev. C **68**, 051601 (2003).
[11] E. Ramakrishnan *et al*., Phys. Rev. C **57**, 1803 (1998).
[12] D. V. Shetty *et al*., Phys. Rev. C **68**, 021602 (2003).
[13] J. P. Bondorf *et al*., Phys. Rep. **257**, 133 (1995).
[14] S. Albergo, S. Costa, E. Costanzo, and A. Rubbino, Nuovo Cimento **A89**, 1 (1985).
[15] J. Randrup and S. Koonin, Nucl. Phys. **A356**, 223 (1981).
[16] A. S. Botvina *et al*., Nucl. Phys. **A475**, 663 (1987).
[17] V. Baran, M. Colonna, M. Di Toro, V. Greco, M. Zielinska Pfabe, and H. H. Wolter, Nucl. Phys. **A703**, 603 (2002).
[18] S. Hudan *et al*., Phys. Rev. C **67**, 064613 (2003).
[19] B. Hong *et al*., Phys. Rev. C **57**, 244 (1998).
[20] T. X. Liu *et al*., Phys. Rev. C **69**, 014603 (2004).
[21] J. B. Natowitz *et al*., Phys. Rev. C **65**, 034618 (2002).
[22] A. S. Botvina, A. B. Larionov, and I. N. Mishustin, Phys. Atom. Nuclei **58**, 1703 (1995).